

Spin-Orbit Semimetal SrIrO₃ in the Two-Dimensional Limit

D. J. Groenendijk,^{1,*} C. Autieri,² J. Girovsky,¹ M. Carmen Martinez-Velarte,¹ N. Manca,¹ G. Mattoni,¹
A. M. R. V. L. Monteiro,¹ N. Gauquelin,³ J. Verbeeck,³ A. F. Otte,¹ M. Gabay,⁴ S. Picozzi,² and A. D. Caviglia¹

¹Kavli Institute of Nanoscience, Delft University of Technology, P.O. Box 5046, 2600 GA Delft, Netherlands

²Consiglio Nazionale delle Ricerche CNR-SPIN, UOS L'Aquila, Sede Temporanea di Chieti, 66100 Chieti, Italy

³Electron Microscopy for Materials Science (EMAT), University of Antwerp, 2020 Antwerp, Belgium

⁴Laboratoire de Physique des Solides, Bat 510, Université Paris-Sud, 91405 Orsay, France

(Received 23 June 2017; published 22 December 2017)

We investigate the thickness-dependent electronic properties of ultrathin SrIrO₃ and discover a transition from a semimetallic to a correlated insulating state below 4 unit cells. Low-temperature magneto-conductance measurements show that spin fluctuations in the semimetallic state are significantly enhanced while approaching the transition point. The electronic properties are further studied by scanning tunneling spectroscopy, showing that 4 unit cell SrIrO₃ is on the verge of a gap opening. Our density functional theory calculations reproduce the critical thickness of the transition and show that the opening of a gap in ultrathin SrIrO₃ requires antiferromagnetic order.

DOI: 10.1103/PhysRevLett.119.256403

Through interface and strain engineering it is possible to tailor the delicate balance between competing energy scales and control the ground state of complex oxides [1,2]. In the two-dimensional (2D) limit, the coordination of constituent ions at the interfaces is reduced, typically yielding a decrease of the electronic bandwidth W . At a critical thickness depending on the relative magnitude of W and the Coulomb repulsion U , a metal-insulator transition can occur [3]. This approach has been applied to study the dimensionality-driven metal-insulator transition (MIT) in 3d transition metal oxides such as SrVO₃ and LaNiO₃, where a transition from a bulklike correlated metallic phase to a Mott or static ordered insulating phase occurs in the 2D limit [1,4–6].

In this Letter, we consider the 5d oxide SrIrO₃ which, in the three-dimensional limit, is a narrow-band semimetal bordering a Mott transition due to a combination of strong spin-orbit coupling (SOC) and electron correlations [7]. We find that an MIT occurs at a film thickness of 4 unit cells (u.c.) and study the evolution of the electronic structure across the transition by (magneto)transport and scanning tunneling spectroscopy (STS). The paramagnetic susceptibility is strongly enhanced while approaching the transition point, which is indicative of the opening of a Mott gap and the concomitant enhancement of magnetic order [8]. Our first-principles density functional theory (DFT) calculations reproduce the critical thickness of the transition and show that the insulating state in the 2D limit is antiferromagnetically ordered. Our study highlights ultrathin SrIrO₃ as a novel platform for engineering the interplay of magnetism and SOC at oxide interfaces.

SrIrO₃ ($n = \infty$) is the only (semi-) metallic member of the Ruddlesden-Popper (RP) series of strontium iridates Sr_{*n*+1}Ir_{*n*}O_{3*n*+1}. On the other end of the series, 2D Sr₂IrO₄

($n = 1$) is a Mott insulator with canted antiferromagnetic order. Despite the extended 5d orbitals, narrow, half-filled $J_{\text{eff}} = 1/2$ bands emerge due to the strong SOC (~ 0.4 eV) and even a relatively small $U \sim 0.5$ eV is sufficient to induce a spin-orbit Mott ground state [9,10]. In SrIrO₃, the effective electronic correlations are smaller due to the three-dimensional corner-sharing octahedral network [11], but the strong SOC causes a significant reduction of the density of states (DOS) at the Fermi level. Together with octahedral rotations that reduce the crystal symmetry, this places the material at the border of a Mott transition and gives rise to an exotic semimetallic state [7,12].

To study changes in electronic structure between the two end members of the RP series, previous studies have focused on varying the number of SrIrO₃ layers in [(SrIrO₃)_{*m*}, SrTiO₃] superlattices [13–17]. While these superlattices closely resemble the RP series, they are distinctly different from SrIrO₃ thin films since they are affected by interlayer coupling. In particular, the superlattices are affected by additional hopping channels and magnetic coupling between SrIrO₃ layers, which gives rise to a reduction of electronic correlations and the appearance of a net in-plane ferromagnetic moment [14,15]. This was recently underlined by Hao *et al.* by demonstrating that the interlayer coupling can be tuned through the number of SrTiO₃ u.c. [16]. By studying single ultrathin SrIrO₃ layers of different thicknesses, we directly address the effect of dimensionality and access the intrinsic properties of 2D SrIrO₃, which forms a building block for spin-orbit coupled superlattices and heterostructures.

A series of SrIrO₃ films with thicknesses between 30 and 2 u.c. were grown by pulsed laser deposition on TiO₂-terminated SrTiO₃(001) substrates. As described in previous work, we use a SrTiO₃ cap layer to prevent film

degradation in ambient conditions and enable lithographic processing [18]. Hall bars were patterned by *e*-beam lithography, and the SrIrO₃ layer was contacted by Ar etching and *in situ* deposition of Pd and Au, resulting in Ohmic contacts. Uncapped SrIrO₃ films were transferred in an N₂ atmosphere from the PLD chamber to the low-temperature scanning tunneling microscopy (STM) setup. More details regarding the growth and sample characterization can be found in the Supplemental Material [19] and in Ref. [18]. First-principles DFT calculations were performed within the generalized gradient approximation using the plane wave VASP [25] package and PBEsol for the exchange-correlation functional [26] with SOC. The Hubbard *U* effects on the Ir and Ti sites were included. To find a unique value of the Coulomb repulsion for the Ir 5*d* states, *U* was tuned in order to reproduce the experimental semimetallic behavior at 4 u.c., while we used $J_H = 0.15U$. Using this approach we obtained $U = 1.50$ eV, which is in good agreement with the typical values used for weakly correlated Ir compounds [27].

Figure 1(a) shows an optical image of a Hall bar used for transport measurements. A high-angle annular dark field scanning transmission electron microscopy (HAADF STEM) image of a 10 u.c. SrIrO₃ film is shown in panel (b), where atomically sharp interfaces with the substrate and the cap layer are visible. The sheet resistance *R* versus temperature *T* of SrIrO₃ films with thicknesses *t* from 30 to 2 u.c. is shown in Fig. 1(c). As the film thickness is reduced, *R* continuously increases and two different regimes can be identified. For $t \geq 4$ u.c., the sheet resistance values are

below 25 kΩ and the films show metallic behavior. Thinner films ($t < 4$ u.c.) have a sheet resistance above 25 kΩ and display insulating behavior. Hence, it is apparent that SrIrO₃ films undergo a semimetal-insulator transition between 4 and 3 u.c., occurring when the sheet resistance crosses $h/e^2 = 25$ kΩ. This is in good agreement with photoemission measurements, which show the disappearance of the Fermi cutoff below 4 u.c. and the opening of a charge gap [28]. In two dimensions, the resistance value h/e^2 corresponds to the limit $k_F l_e \sim 1$, where k_F is the Fermi wave vector and l_e is the mean free path, marking the transition from weak to strong localization [29].

In the (semi-) metallic ($t \geq 4$ u.c.) regime, the films show bad metallic behavior in the high temperature range, consistent with previous reports [18,30,31]. The resistance first decreases linearly with temperature until T_{\min} , below which an upturn occurs. In addition, the residual resistance ratio defined as $R(300 \text{ K})/R(T_{\min})$ is rather low for all thicknesses (~ 1.2). Such anomalous metallic behavior is often observed in materials that are bordering a Mott transition. Upon decreasing the film thickness from 30 to 4 u.c., T_{\min} increases from 10 to 60 K [Fig. 1(c), inset]. In the semimetallic regime, the resistivity curves $\rho(T)$ collapse [Fig. 1(d)] and display similar behavior apart from the increasingly strong upturn at low temperature. Interestingly, the resistance upturn is accompanied by an increase of the Hall coefficient R_H [19], which is likely related to the semimetallic electronic structure as underscored by ARPES measurements [7,32]. Since the top energy of several hole bands was measured to lie just below the Fermi level, these bands will be progressively depopulated with decreasing temperature, increasing R_H and the resistance.

Transport in ultrathin films ($t < 4$ u.c.) occurs in a strongly localized regime with a sheet resistance well in excess of h/e^2 . For the 3 u.c. film, the conductivity σ can be well described by a variable range hopping (VRH) type of conduction. In this case, electrons hop between localized states and the conductance is given by $\sigma = C \exp[-(T_0/T)^\alpha]$, where T_0 depends on the density of localized states and the spread of their wave functions [33]. VRH conductivity can be of either Mott or Efros-Shklovskii type, which for a 2D system translates into exponents $\alpha = 1/3$ and $1/2$, respectively [34]. The fit to the data yields an exponent $\alpha = 0.57$, which is in good agreement with the latter, suggesting the existence of a Coulomb gap. On the other hand, the 2 u.c. film follows Arrhenius-type behavior where $R \propto \exp(E_g/2k_B T)$, which yields an energy gap E_g of approximately 95 meV.

To probe changes in the electronic structure and spin relaxation while approaching the transition point, we perform magnetotransport measurements. Figure 2(a) shows the out-of-plane magnetoconductance $\Delta\sigma$ in units of $e^2/\pi h$ measured at 1.5 K for film thicknesses from 30 to 4 u.c. In the limit of large thickness, the magnetoconductance is negative and quadratic and displays a cusp around

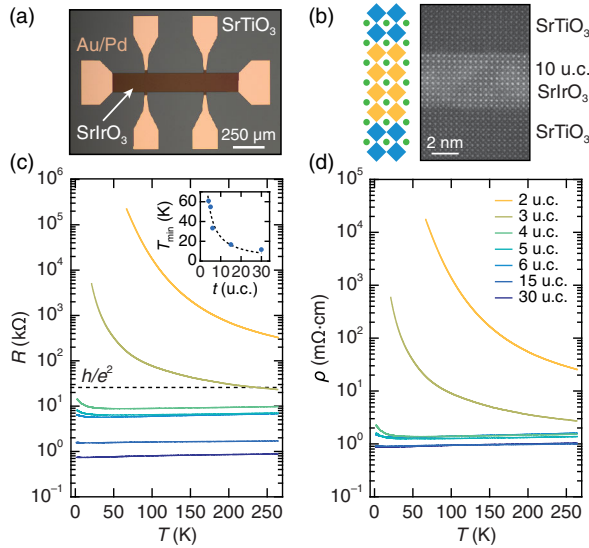


FIG. 1. (a) Optical image of a Hall bar used for transport measurements. (b) HAADF-STEM image of a SrTiO₃/10 u.c. SrIrO₃/SrTiO₃ heterostructure. (c) $R(T)$ and (d) $\rho(T)$ curves for films of different thicknesses. The inset shows the temperature of the resistance minimum (T_{\min}) as a function of thickness.

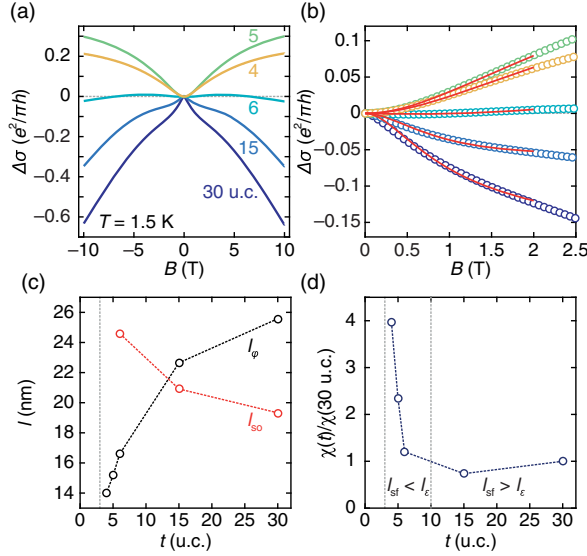


FIG. 2. (a) Magnetoconductance $\Delta\sigma = \sigma(B) - \sigma(0)$ in units of $e^2/\pi h$ measured in an out-of-plane magnetic field for films of different thicknesses. (b) $\Delta\sigma$ fitted by the Maekawa-Fukuyama formula (solid red lines). (c) l_{so} and l_ϕ extracted from the fits. (d) Relative susceptibility $\chi(t)/\chi(30 \text{ u.c.})$ versus thickness.

$B = 0$ T as reported in other works [30,31]. However, a crossover from negative to positive values occurs as we approach the MIT. We attribute this behavior to weak (anti-) localization, the interference of quantum coherent electronic waves undergoing diffusive motion (in the presence of SOC). To investigate this scenario, we fit the curves with the Maekawa-Fukuyama formula [red lines in Fig. 2(b)] in a diffusive regime that describes the change in the conductivity with magnetic field with negligible Zeeman splitting [35]. The extracted parameters B_ϕ and B_{so} are the effective fields related to the inelastic and spin-orbit relaxation lengths, respectively.

Since all the films have similar resistivity values, we fix B_e to 1.2 T, corresponding to an elastic length of approximately 11.7 nm and a carrier density in the order of 10^{19} cm^{-3} . This value yields the best fits over the entire thickness range (see Ref. [19]) and is consistent with a Drude contribution. For the 30, 15, and 6 u.c. films, a B^2 component was fitted at high fields and subtracted to account for the classical orbital magnetoconductance [19]. The scattering lengths l_i are related to the effective fields by $B_i = \hbar/4el_i^2$, and their fitted values are shown in Fig. 2(c). The extracted lengths show a crossover from $l_\phi > l_{so}$ for the thicker samples (30, 15 u.c.) to $l_\phi < l_{so}$ for the thinner ones (6, 5, 4 u.c.), capturing the crossover from negative (weak antilocalization) to positive (weak localization) magnetoconductance as the film thickness is reduced.

A close look at the thickness dependence of l_ϕ reveals deviations from the expected behavior considering only electron-electron corrections to the weak localization

expression ($1/l_e^2 \sim R \log k_F l_e$, where l_e is the length associated with electron-electron corrections). To correctly describe the physics at play, one needs to include diffusive spin fluctuations which, when sufficiently large, can set the inelastic scattering length, leading to an effective inelastic scattering time given by $1/\tau_\phi = 1/\tau_e + 2/3\tau_{SF}$, where τ_ϕ is related to the energy relaxation time τ_e and to the spin-fluctuation time τ_{SF} ($l_i^2 = D\tau_i$, where D is the diffusion constant) [36]. Since $1/l_{SF}^2$ is proportional to the paramagnetic susceptibility $\chi(t)$, we can qualitatively track the variation of χ by studying the thickness dependence of l_ϕ . Figure 2(d) shows the relative susceptibility $\chi(t)/\chi(30 \text{ u.c.})$ as a function of thickness. The increase of χ at low thicknesses is characteristic of a magnetic transition. We note that the transition from negative to positive magnetoconductance is set by the relative magnitude of l_e and l_{SF} . Near the transition point, $l_{SF} < l_e$, i.e., spin fluctuations are large, leading to a positive magnetoconductance due to weak localization. In the limit of large thickness, $l_{SF} > l_e$, l_{so} . Here, both electron-electron interactions and weak antilocalization contribute to the negative magnetoconductance. Structural studies have shown that octahedral coupling at the $\text{SrTiO}_3/\text{SrIrO}_3$ interface suppresses the bulk octahedral rotations in the SrIrO_3 film for $t < 4$ u.c., enhancing magnetic interactions [28]. Within this view, the increase of χ as the film thickness is reduced can be understood as an increased fractional contribution from the less distorted magnetic interfacial region.

Further insights into the anomalous behavior in the semimetallic state and the electronic structure near the MIT are obtained by measuring the local DOS across the Fermi energy E_F by STS measurements. A topographic STM image [inset Fig. 3(a)] acquired on a 10 u.c. SrIrO_3 film shows terraces and steps with height equal to 1 u.c., indicating a layer-by-layer growth mode and showing that the surface is single terminated. Figure 3(a) shows differential conductance (dI/dV) spectra acquired at 4 K on films

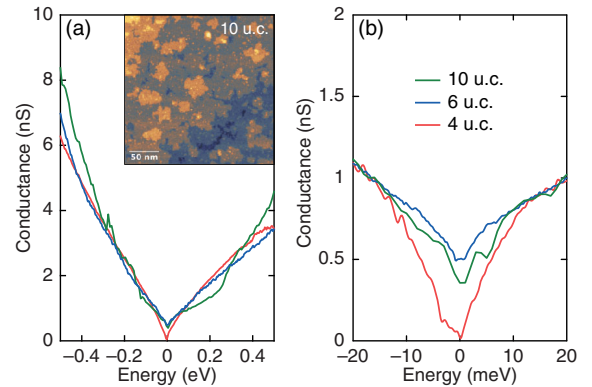


FIG. 3. (a) Differential conductance (dI/dV) spectra acquired on three different samples with film thicknesses of 4, 6, and 10 u.c.. Inset: STM topographic image of the surface of a 10 u.c. SrIrO_3 film. (b) dI/dV spectra measured in a smaller energy range.

of 4, 6, and 10 u.c. thickness. The spectra show V-shaped behavior with a linear dependence of the DOS for both occupied and unoccupied states. As shown in Fig. 3(b), the minimum of the spectra is at zero energy (i.e., at E_F) for all thicknesses, and while the spectra taken on the 6 and 10 u.c. films exhibit finite DOS, the 4 u.c. sample shows zero DOS at E_F . Therefore, the evolution of the DOS at E_F reflects the approach of the MIT, where the 4 u.c. film is on the verge of a gap opening.

V-shaped differential conductance spectra have previously been observed in (i) systems with 2D Dirac surface states such as germanene/Pt(111) and graphene/SiC [37,38] and (ii) in the pseudogap phase of doped Mott insulators such as cuprates [39,40]. A Dirac cone is not expected in this system due to the breaking of n -glide symmetry by epitaxial constraint, as was shown previously for SrIrO₃ on GdScO₃ [41,42]. However, in a recent work similar V-shaped behavior was found for Sr₂IrO₄ doped with La³⁺, showing zero DOS at E_F [43]. This observation was explained as being a result of charge carriers becoming untrapped for La concentrations exceeding 4%. The resemblance between the two systems could stem from both SrIrO₃ and doped Sr₂IrO₄ being in close proximity to a metal-insulator transition, although on opposite sides of the phase boundary. However, further investigation is required to fully address the exact nature of the V-shaped DOS of SrIrO₃ thin films.

To study the electronic and magnetic structure of SrIrO₃ in the 2D limit, we perform first-principles calculations. We first consider how the properties of bulk SrIrO₃ evolve as a function of U . At low U , the system shows a nonmagnetic metallic state topologically protected by time-reversal symmetry [44]. Upon increasing U , a canted G -type antiferromagnetic (AFM) metallic state with a net in-plane magnetic moment emerges [14]. A further increase of U opens a gap, leading to a G -type AFM insulating state [45] like in [(SrIrO₃) _{m} , SrTiO₃] superlattices [14]. Since both U and the breaking of time-reversal symmetry are required to open the gap, insulating SrIrO₃ is located in the intermediate region between a Slater- and a Mott-type insulator. The same qualitative results were obtained in other Ir compounds [46,47].

When moving from bulk SrIrO₃ to SrIrO₃/SrTiO₃ heterostructures, compressive strain, reduction of the bandwidth and an increase of U have to be taken into account. Compressive strain ($\sim 1\%$) favors the metallicity [13] because of the increased bandwidth [27]. The other two effects favor the insulating state [48] and are needed to observe the semimetallic or insulating phase in SrIrO₃ ultrathin films. We note that U is typically larger in thin films than in superlattices since in the latter the SrIrO₃ layers are expected to exhibit a relaxation of octahedral tilts towards bulk values facilitated by tilts in the SrTiO₃ layers [49]. For our calculations we focused on the thickness range in the vicinity of the MIT and computed the band

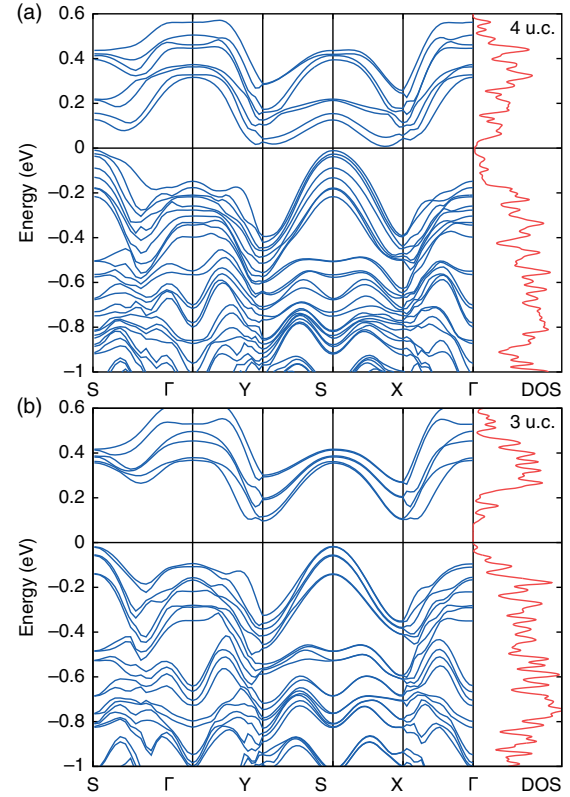


FIG. 4. Calculated electronic structure for (a) 4 and (b) 3 u.c. SrIrO₃ films on tetragonal SrTiO₃ with $U = 1.50$ eV. Right: the corresponding DOS per formula unit as a function of energy.

structure of 3 and 4 u.c. SrIrO₃ layers on a SrTiO₃ substrate in the slab geometry (including vacuum) for $U = 1.50$ eV [19]. The results are shown together with the corresponding DOS in Figs. 4(a) and 4(b), respectively.

The bandwidth reduction when going from 4 to 3 u.c. results in a localization of the carriers, and triggers a transition from a semimetallic to an AFM insulating state. Even for a single layer of SrIrO₃ on SrTiO₃ the nonmagnetic case is found to be metallic, and AFM ordering is required for the opening of a gap [28]. The electronic structure of the 4 u.c. film shows a gap-closing behavior, consistent with STS. In the case of 3 u.c. the gap is 60 meV; its precise value is, however, crucially dependent on many effects such as octahedral distortions, magnetic order, strain, connectivity, and Coulomb repulsion. Near the Fermi level, the DOS is dominated by a $5d t_{2g}$ contribution as in bulk SrIrO₃. Hence, by reducing the thickness, we approach a state closer to $J_{\text{eff}} = 1/2$ as in Sr₂IrO₄. However, while the t_{2g} unoccupied bandwidth is comparable to Sr₂IrO₄, the occupied part shows a mixed $J_{\text{eff}} = 1/2, 3/2$ behavior rather than a pure $J_{\text{eff}} = 1/2$ picture.

In conclusion, we have shown that SrIrO₃ can be driven into a correlated insulating state in the 2D limit. Quantum corrections to the conductivity indicate significant changes in scattering mechanisms in the semimetallic regime near the transition point. The divergence of χ is indicative of the

opening of a Mott gap and the concomitant enhancement of magnetic order. The close proximity of SrIrO_3 to a correlated insulating state is further corroborated by STS measurements, showing a V-shaped DOS similar to the doped $J_{\text{eff}} = 1/2$ Mott insulator Sr_2IrO_4 . In addition, the 4 u.c. film reflects the onset of the gap opening as it shows zero DOS at the E_F , being at the border of the MIT. Our DFT calculations reproduce the metal-insulator transition for $U = 1.50$ eV and show that antiferromagnetism develops concomitantly with the opening of a gap.

This work was supported by The Netherlands Organisation for Scientific Research (NWO/OCW) as part of the Frontiers of Nanoscience program (NanoFront), by the Dutch Foundation for Fundamental Research on Matter (FOM), and by the European Research Council under the European Union's H2020 programme/ERC Grant Agreement No. [677458]. The authors thank R. Claessen, P. Schütz, D. Di Sante, G. Sangiovanni, and A. Santander Syro for useful discussions. M. G. gratefully acknowledges support from the French National Research Agency (ANR) (Project LACUNES No. ANR-13-BS04-0006-01). C. A. and S. P. acknowledge financial support from Fondazione Cariplo via the project Magister (Project No. 2013-0726) and from CNR-SPIN via the Seed Project "CAMEO". N. G. and J. V. acknowledge support from the GOA project "Solarpaint" of the University of Antwerp. The Qu-Ant-EM microscope was partly funded by the Hercules fund from the Flemish Government.

*d.j.groenendijk@tudelft.nl

- [1] K. Yoshimatsu, T. Okabe, H. Kumigashira, S. Okamoto, S. Aizaki, A. Fujimori, and M. Oshima, *Phys. Rev. Lett.* **104**, 147601 (2010).
- [2] P. Zubko, S. Gariglio, M. Gabay, P. Ghosez, and J.-M. Triscone, *Annu. Rev. Condens. Matter Phys.* **2**, 141 (2011).
- [3] J. Hubbard, *Proc. R. Soc. A* **276**, 238 (1963).
- [4] A. V. Boris, Y. Matiks, E. Benckiser, A. Frano, P. Popovich, V. Hinkov, P. Wochner, M. Castro-Colin, E. Detemple, V. K. Malik, C. Bernhard, T. Prokscha, A. Suter, Z. Salman, E. Morenzoni, G. Cristiani, H.-U. Habermeier, and B. Keimer, *Science* **332**, 937 (2011).
- [5] P. D. C. King, H. I. Wei, Y. F. Nie, M. Uchida, C. Adamo, S. Zhu, X. He, I. Božović, D. G. Schlom, and K. M. Shen, *Nat. Nanotechnol.* **9**, 443 (2014).
- [6] R. Scherwitzl, S. Gariglio, M. Gabay, P. Zubko, M. Gibert, and J.-M. Triscone, *Phys. Rev. Lett.* **106**, 246403 (2011).
- [7] Y. F. Nie, P. D. C. King, C. H. Kim, M. Uchida, H. I. Wei, B. D. Faeth, J. P. Ruf, J. P. C. Ruff, L. Xie, X. Pan *et al.*, *Phys. Rev. Lett.* **114**, 016401 (2015).
- [8] M. Imada, A. Fujimori, and Y. Tokura, *Rev. Mod. Phys.* **70**, 1039 (1998).
- [9] B. J. Kim, H. Jin, S. J. Moon, J.-Y. Kim, B.-G. Park, C. S. Leem, J. Yu, T. W. Noh, C. Kim, S.-J. Oh *et al.*, *Phys. Rev. Lett.* **101**, 076402 (2008).
- [10] B. J. Kim, H. Ohsumi, T. Komesu, S. Sakai, T. Morita, H. Takagi, and T. Arima, *Science* **323**, 1329 (2009).
- [11] J. K. Kawasaki, M. Uchida, H. Paik, D. G. Schlom, and K. M. Shen, *Phys. Rev. B* **94**, 121104 (2016).
- [12] I. Pallecchi, M. T. Buscaglia, V. Buscaglia, E. Gilioli, G. Lamura, F. Telesio, M. R. Cimberle, and D. Marré, *J. Phys. Condens. Matter* **28**, 065601 (2016).
- [13] K.-H. Kim, H.-S. Kim, and M. J. Han, *J. Phys. Condens. Matter* **26**, 185501 (2014).
- [14] J. Matsuno, K. Ihara, S. Yamamura, H. Wadati, K. Ishii, V. V. Shankar, H.-Y. Kee, and H. Takagi, *Phys. Rev. Lett.* **114**, 247209 (2015).
- [15] S. Y. Kim, C. H. Kim, L. J. Sandilands, C. H. Sohn, J. Matsuno, H. Takagi, K. W. Kim, Y. S. Lee, S. J. Moon, and T. W. Noh, *Phys. Rev. B* **94**, 245113 (2016).
- [16] L. Hao, D. Meyers, C. Frederick, G. Fabbri, J. Yang, N. Traynor, L. Horak, D. Kriegner, Y. Choi, J.-W. Kim, D. Haskel, P. J. Ryan, M. P. M. Dean, and J. Liu, *Phys. Rev. Lett.* **119**, 027204 (2017).
- [17] D. Meyers, Y. Cao, G. Fabbri, N. J. Robinson, L. Hao, C. Frederick, N. Traynor, J. Yang, J. Lin, M. Upton *et al.*, [arXiv:1707.08910](https://arxiv.org/abs/1707.08910).
- [18] D. J. Groenendijk, N. Manca, G. Mattoni, L. Kootstra, S. Gariglio, Y. Huang, E. van Heumen, and A. D. Caviglia, *Appl. Phys. Lett.* **109**, 041906 (2016).
- [19] See Supplemental Material at <http://link.aps.org/supplemental/10.1103/PhysRevLett.119.256403> for additional information on film characterization, (magneto)transport measurements and first-principles calculations, which includes Refs. [20–24].
- [20] P. E. Blöchl, *Phys. Rev. B* **50**, 17953 (1994).
- [21] H. J. Monkhorst and J. D. Pack, *Phys. Rev. B* **13**, 5188 (1976).
- [22] V. I. Anisimov, J. Zaanen, and O. K. Andersen, *Phys. Rev. B* **44**, 943 (1991).
- [23] A. I. Liechtenstein, V. I. Anisimov, and J. Zaanen, *Phys. Rev. B* **52**, R5467 (1995).
- [24] E. Pavarini, S. Biermann, A. Poteryaev, A. I. Liechtenstein, A. Georges, and O. K. Andersen, *Phys. Rev. Lett.* **92**, 176403 (2004).
- [25] G. Kresse and D. Joubert, *Phys. Rev. B* **59**, 1758 (1999).
- [26] J. P. Perdew, A. Ruzsinszky, G. I. Csonka, O. A. Vydrov, G. E. Scuseria, L. A. Constantin, X. Zhou, and K. Burke, *Phys. Rev. Lett.* **100**, 136406 (2008).
- [27] B. Kim, P. Liu, and C. Franceschini (to be published).
- [28] P. Schütz, D. D. Sante, L. Dudy, J. Gabel, M. Stübinger, M. Kamp, Y. Huang, M. Capone, M.-A. Husanu, V. Strocov, G. Sangiovanni, M. Sing, and R. Claessen, following Letter, *Phys. Rev. Lett.* **119**, 256404 (2017).
- [29] D. C. Licciardello and D. J. Thouless, *Phys. Rev. Lett.* **35**, 1475 (1975).
- [30] A. Biswas, K.-S. Kim, and Y. H. Jeong, *J. Appl. Phys.* **116**, 213704 (2014).
- [31] L. Zhang, Q. Liang, Y. Xiong, B. Zhang, L. Gao, H. Li, Y. B. Chen, J. Zhou, S.-T. Zhang, Z.-B. Gu *et al.*, *Phys. Rev. B* **91**, 035110 (2015).
- [32] Z. T. Liu, M. Y. Li, Q. F. Li, J. S. Liu, W. Li, H. F. Yang, Q. Yao, C. C. Fan, X. G. Wan, Z. Wang *et al.*, *Sci. Rep.* **6**, 30309 (2016).

- [33] W. Brenig, G. H. Döhler, and H. Heyszenau, *Philos. Mag.* **27**, 1093 (1973).
- [34] R. Rosenbaum, *Phys. Rev. B* **44**, 3599 (1991).
- [35] S. Hurand, A. Jouan, C. Feuillet-Palma, G. Singh, J. Biscaras, E. Lesne, N. Reyren, A. Barthélémy, M. Bibes, J. E. Villegas *et al.*, *Sci. Rep.* **5**, 12751 (2015).
- [36] S. Maekawa and H. Fukuyama, *J. Phys. Soc. Jpn.* **50**, 2516 (1981).
- [37] C. J. Walhout, A. Acun, L. Zhang, M. Ezawa, and H. J. W. Zandvliet, *J. Phys. Condens. Matter* **28**, 284006 (2016).
- [38] Y. J. Song, A. F. Otte, Y. Kuk, Y. Hu, D. B. Torrance, P. N. First, W. A. de Heer, H. Min, S. Adam, M. D. Stiles *et al.*, *Nature (London)* **467**, 185 (2010).
- [39] Y. Kohsaka, K. Iwaya, S. Satow, T. Hanaguri, M. Azuma, M. Takano, and H. Takagi, *Phys. Rev. Lett.* **93**, 097004 (2004).
- [40] P. Cai, W. Ruan, Y. Peng, C. Ye, X. Li, Z. Hao, X. Zhou, D.-H. Lee, and Y. Wang, *Nat. Phys.* **12**, 1047 (2016).
- [41] J. Liu, D. Kriegner, L. Horak, D. Puggioni, C. R. Serrao, R. Chen, D. Yi, C. Frontera, V. Holy, A. Vishwanath *et al.*, *Phys. Rev. B* **93**, 085118 (2016).
- [42] J.-M. Carter, V. V. Shankar, M. A. Zeb, and H.-Y. Kee, *Phys. Rev. B* **85**, 115105 (2012).
- [43] I. Battisti, K. M. Bastiaans, V. Fedoseev, A. De La Torre, N. Iliopoulos, A. Tamai, E. C. Hunter, R. S. Perry, J. Zaanen, F. Baumberger *et al.*, *Nat. Phys.* **13**, 21 (2016).
- [44] H.-S. Kim, Y. Chen, and H.-Y. Kee, *Phys. Rev. B* **91**, 235103 (2015).
- [45] M. A. Zeb and H.-Y. Kee, *Phys. Rev. B* **86**, 085149 (2012).
- [46] X. Ming, K. Yamauchi, T. Oguchi, and S. Picozzi, *arXiv*: 1702.04408.
- [47] H. Watanabe, T. Shirakawa, and S. Yunoki, *Phys. Rev. B* **89**, 165115 (2014).
- [48] C. Autieri, *J. Phys. Condens. Matter* **28**, 426004 (2016).
- [49] J. Hwang, J. Son, J. Y. Zhang, A. Janotti, C. G. Van de Walle, and S. Stemmer, *Phys. Rev. B* **87**, 060101 (2013).